Inflation Response of Peripapillary Retina during Acute Intraocular Pressure Elevation

Sunny Kwok, MS[1], Manqi Pan[1], Yanhui Ma, PhD[1,2], Xueliang Pan, PhD[3], Nicholas Hazen, MS[1,4], and Jun Liu, PhD[1,2,4*]

[1] Department of Biomedical Engineering, The Ohio State University, Columbus, OH

[2] Department of Ophthalmology and Visual Science, The Ohio State University, Columbus, OH

[3] Department of Biomedical Informatics, The Ohio State University, Columbus, OH

[4] Biophysics Interdisciplinary Group, The Ohio State University, Columbus, OH

* Corresponding author – email: liu.314@osu.edu

Abstract

Purpose: In the disease of glaucoma, elevated intraocular pressure (IOP) may mechanically damage retina tissue leading to vision loss. The mechanical deformation of retina during IOP elevations have not been well-characterized. We aim to characterize the peripapillary retina (PPR) deformation during IOP elevation in human donor eyes using high-frequency ultrasound elastography. **Methods:** Whole globe inflation was performed in ten donor eyes (age: 20-74 years old) while IOP was raised from 5 to 30 mmHg. High-frequency ultrasound scans of the posterior eye centered at the optic nerve head (ONH) were collected during inflation. A correlation-based speckle tracking algorithm was used to compute displacements, and tissue strains were calculated using least-squares estimation. Radial, tangential, and shear strains were mapped for manually segmented regions of interest (PPR and peripapillary sclera (PPS)). **Results:** Our results showed that PPR experienced high shear strain, less radial strain, and low tangential strain at 30 mmHg. Localized high shear and tangential strains were present throughout PPR. In comparison to PPS, PPR had greater shear, less radial compression, and similar levels of tangential stretch. **Conclusion:** Peripapillary retinal damage is characteristic of glaucoma progression. Our findings suggest that although PPR experienced minimal radial compression during IOP elevation, high shear could contribute to mechanical damage of neural tissue during IOP elevation. These results provide new insights into IOP-related mechanical insults on neural tissue near the ONH, where glaucomatous damage initiates.

Keywords: glaucoma, ocular biomechanics, retina, high-frequency ultrasound, ultrasound elastography

1. Introduction

The retina is a light-sensitive layer of neural tissue in the eye that plays an essential role in the visual pathway. Incoming light energy is converted to electrochemical signals that are passed along the retinal nerve fiber layer (RNFL) to the optic nerve head (ONH), where the nerve axons converge and exit the eye. In the group of diseases known as glaucoma, damage to these optic nerve axons lead to severe vision loss and blindness. Elevated intraocular pressure (IOP) has been identified as a primary risk factor for glaucoma onset and progression. As such, IOP-related mechanical damage to ONH neural tissue plays a central role in glaucoma pathophysiology. Therefore, characterization of the deformation response of the peripapillary tissues surrounding the ONH in response to IOP elevation may further our understanding of the biomechanical contributors to glaucoma damage.

The fragile nature of the retina has limited the extent of its biomechanical characterization. In ex vivo mechanical testing, controlled attachment of the delicate tissue samples to testing apparatus was a commonly reported challenge. Using synthetic adhesives, a few early uniaxial tensile studies in animal models showed the retina is resistant to in-plane stretch with a stress-strain response akin to plastic deformation [1,2]. Other studies using tensile tests showed a variable tensile modulus in retina that was dependent on temperature and structural differences between regions [3–5]. More recently, efforts have been made to measure retinal compressive properties that better describe its behavior under the physiological loading of IOP. It has been shown that retina's compressive modulus was about 10 times lower than its tensile modulus [6]. Elastography methods using imaging modalities such as Optic Coherence Tomography (OCT) [7–9] and ultrasound [10,11] have also been applied to characterize retinal deformation in whole eye models under physiological loads. However, few studies have reported the deformation response of the peripapillary retina in the region surrounding the ONH during IOP elevations.

The primary objective of the present study was to characterize the deformation of the human peripapillary retina (PPR) in response to acute IOP elevations. High-frequency ultrasound offers excellent tissue penetration and spatial resolution for imaging the structures in and around the ONH. We have developed and validated a technique applying high frequency ultrasound to measure tissue deformation in the posterior eye and reported ONH and peripapillary sclera (PPS) strains during IOP elevation [12–15]. Using this technique, we measured the PPR deformation in normal and glaucomatous eyes and compared it with PPS deformation to gain insights into the biomechanical response of this critical ONH tissue structure during acute IOP elevation. The results from this study may further the understanding of the potential mechanical alterations of essential ONH structures in glaucoma.

2. Methods

Donor Information and Experimental Setup

Ten normal donor globes (age: 20 – 74 years; mean ± SD: 49 ± 20; 4 male and 6 female) were obtained from the Lion's Eye Bank of West Central Ohio (Dayton, OH, USA) in accordance with the Declaration of Helsinki. All globes were recovered within 12 hours postmortem and all experiments were completed within 36 hours postmortem. The globes were stored in a moist container at 4°C until experimental use.

Before inflation, extraocular tissue was removed from the globe and the optic nerve was trimmed close to the surface of the sclera for ultrasound imaging from the posterior side. Two spinal needles were inserted through the equator of the globe to secure the eye to a custom-built holder with the ONH facing upward (Fig. 1A). Two 20G needles were inserted into the anterior chamber of the eye, one connected to an infusion pump (Ph.D. Ultra, Harvard Apparatus, MA, USA) and the other to a pressure sensor (P75, Harvard Apparatus) to control and continuously record IOP. The eye was immersed in 0.9% saline to maintain tissue hydration and facilitate ultrasound transduction.

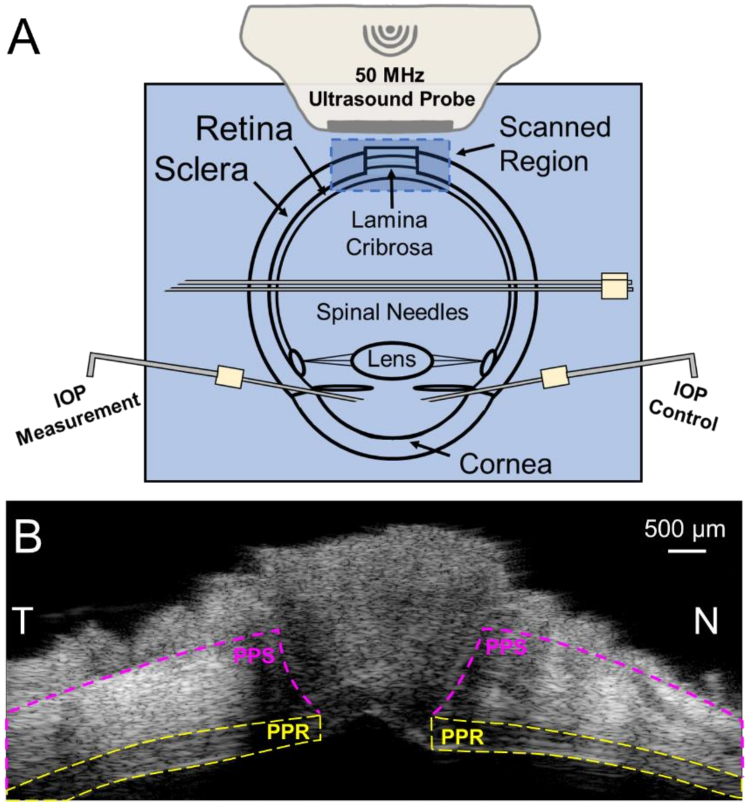

Figure 1: A) Experimental setup of human donor globe inflation with high-frequency ultrasound imaging of the ONH and peripapillary region. B) A representative ultrasound image of the scanned region along the nasal-temporal (NT) axis. PPS (dashed yellow) and PPR (dashed pink) segmentation are shown.

Inflation Testing with Ultrasound Imaging

For all inflation testing, control of the testing apparatus and data acquisition were implemented by using a customized LabView program (National Instruments, Austin, TX, USA). The globes were first preconditioned with 20 cycles from 5 to 30 mmHg at 2 seconds per cycle before equilibrating at 5 mmHg for 30 minutes. The inflation tests were then performed by increasing IOP from 5 to 30 mmHg with 0.5 mmHg steps. The IOP was held constant at each pressure level for 30 seconds before ultrasound scans were acquired using a 50MHz ultrasound probe (MS700, Vevo2100, VisualSonics). Each eye was inflated twice to capture 2D scans (approximately 5 mm × 10 mm) of the posterior eye centered at the ONH along the nasal-temporal (NT) and superior-inferior (SI) axes. Scans were separated by 30 minutes of equilibration time at 5 mmHg in between.

Ultrasound Speckle Tracking Algorithm

A correlation-based ultrasound speckle tracking algorithm has been described and validated previously [12]. Briefly, digitized ultrasound radiofrequency (RF) data, sampled at 1.5 μm × 19 μm (axial × lateral), are acquired during image acquisition. To perform speckle tracking, a region of interest (ROI) was manually defined to include all visible tissue between the boundaries of the PPS and PPR, including the ONH, at the initial IOP. Within the ROI, the RF data are divided into kernels, each containing 51 × 31 pixels (75 μm × 570 μm). A 50% kernel overlap was applied to improve spatial resolution [16]. The displacement of each kernel was computed by cross-correlation between successive RF frames within a search window. The maximum correlation coefficient value designates the new location of the kernel, and spline interpolation allows for subpixel resolution in displacement tracking. The cumulative displacement vectors were calculated with respect to the kernel location at the initial IOP. Strains were calculated using least squares estimation based on the local displacement field gradient [17]. Radial, tangential, and shear strain was obtained by coordinate transformation from Cartesian to the polar coordinates based on the tissue curvature to eliminate the effect of pure rotation and better describes the anatomy of the posterior eye. Color maps were generated to visualize the spatial distribution of the tissue displacements and strains. Strain maps were generated for each region with spline interpolation of the kernels to the pixel level.

Peripapillary Retina Deformation Analysis

For all eyes, PPS and PPR were defined by manual segmentation based on tissue boundaries visible in ultrasound images (Fig 1B). We have previously validated the repeatability of manual segmentation of ONH structures for ultrasound images, showing excellent interobserver repeatability [15]. Choroid was not separable from the sclera in the ultrasound images, and thus was included within the PPS region. Average displacement and strains in each region were obtained and analyzed, only data at 30 mmHg are reported in the text as an example. The differences and correlations of the average strains between the different regions were evaluated by using paired t-tests.

3. Results

Representative ultrasound images of a normal ONH are presented in Figure 1B. High frequency ultrasound captures consistent speckle patterns across the range of experimental IOP as evidenced by the high speckle tracking correlation coefficient (>0.99).

In normal eyes, the average radial, tangential, and shear strains were -2.07±0.65%, 0.38±0.14%, and 1.08±0.32%, respectively. Representative strain maps depicting regional PPR and PPS radial, tangential, and shear strains are shown in Figure 2. At 30 mmHg, PPR had shear strain of 1.46±0.55% that was significantly greater than the radial strain magnitude (-0.79±0.36%, $p=0.004$) and tangential strain (0.40±0.26%, $p<0.001$). In comparison to PPR, PPS had greater radial strain (-2.83±1.03%, $p<0.001$, see Fig. 3A), less shear strain (1.05±0.33%, $p=0.043$), and similar levels of tangential strain (0.46±0.23%, $p=0.575$).

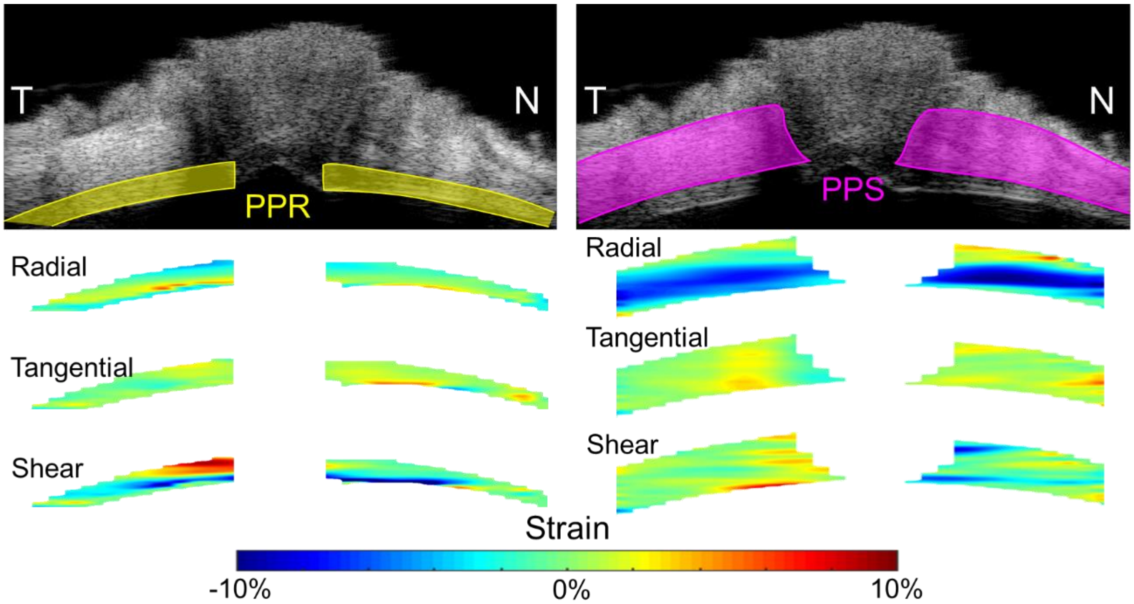

Figure 2: Radial, tangential, and shear strain maps of PPR (left, shaded in yellow) and PPS (right, shaded in pink) from a representative normal eye at 30 mmHg.

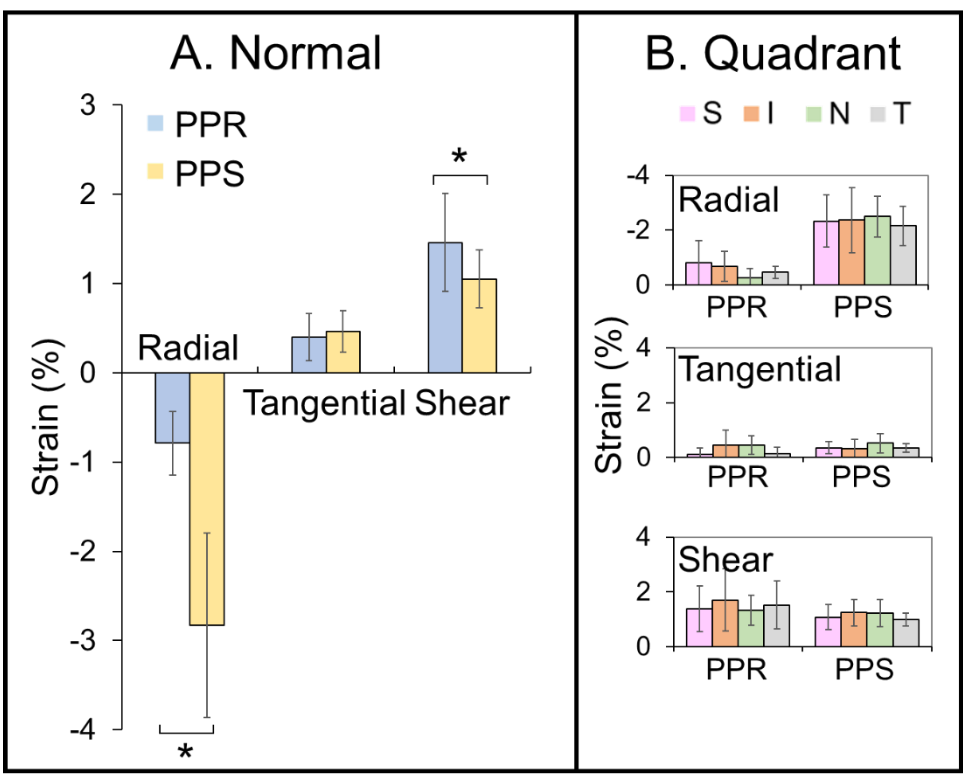

Figure 3: A) Comparisons of the radial, tangential, and shear strains between PPR and PPS at 30 mmHg in normal eyes (* denotes $p<0.05$). B) PPR and PPS strains showed no significant differences across quadrants. S: superior, I: inferior, N: nasal, T: temporal.

Localized high shear strains were observed in PPR in the region close to the ONH (up to 10%, Fig. 2). In some cases, higher tangential strains were also seen in the same location of high shear, especially along the anterior boundary of the PPR. Exploratory analysis showed no significant differences in strains between quadrants in either PPR or PPS (see Fig. 2C).

4. Discussion

In this study, we reported the deformation response of the PPR and PPS during IOP elevation in human donor eyes. Whole eye inflation preserved the structural complexities of the posterior eye which provides an excellent model to explore the mechanical response of ONH structures to IOP changes. The primary findings of this study include:

1. In PPR, the magnitude of shear strains was significantly larger than the magnitude of radial and tangential strains;
2. PPS had significantly greater radial strains, but less shear strains than the PPR;

Interestingly, although the PPS had high radial compression, especially in the more anterior region adjacent to the PPR, PPR itself experienced minimal radial compression during acute IOP rise. Fortune et al. had reported that an acute IOP elevation of 35 mmHg held for an hour had minimal effects on retinal thickness in nonhuman primate models [18]. It is surprising that the retina, which is known to be a compliant tissue, appear to better resist the compressive loading radially than the tougher PPS. At higher IOP, our results suggest that the ability of the PPS to compress may serve as a protection for the neural PPR against large compressive impact during acute IOP rise.

We also observed regions of high shear concentrated near the ONH. Increased shear along the ONH-PPS boundary has been previously reported [14], which may indicate mechanical vulnerability along this boundary to damage from acute loading. Although the overall PPR tangential strain was low, localized high tangential strain was also observed along the anterior surface of PPR in most eyes. This region is significant as it may correspond to the RNFL consisting of axon fibers. Localized high strains could contribute toward mechanical susceptibility in these regions to IOP-related glaucomatous damage.

This study has a few limitations. A small sample size limited our ability to perform a more powered quadrant regional analysis. However, the current sample size was sufficient to discern significant differences in the deformation response of various ONH tissues. Future studies will expand the sample size to validate the current study and to further explore the quadrant-specific deformation responses. The ex vivo inflation model does not fully represent the complexities of the in vivo system. Although several other mechanical stressors such as blood pressure, cerebrospinal fluid pressure, and optic nerve tension exist in and around the ONH, IOP has been shown to be the dominant load affecting ONH stresses and strains [22–25]. This gives us confidence that we captured the most prominent deformation response within this study. Finally, the present study was limited to 2D characterization of ONH tissues along two perpendicular planes. It should be noted that the deformation of the entire posterior volume cannot be simply summarized by two meridians. Our lab has developed a 3D ultrasound imaging technique that would be able to provide a much more comprehensive and accurate characterization of retinal deformation [16,26,27].

Optic neuropathy, most notably within and around the ONH, is characteristic of glaucoma. High-frequency ultrasound elastography has enabled the quantification of mechanical deformations in ONH tissue structures in response to IOP elevations. Within the same eye, comparison of PPR and PPS showed a similar shear response but different radial response in normal eyes. These findings may provide new insights into IOP-related mechanical insults to the neural and connective tissues in and around the ONH, where glaucomatous damage initiates.

5. Acknowledgements:

This work was supported by NIH Grant No. R01EY025358.

References

[1] Wu, W., Peters, W. H., and Hammer, M. E., 1987, “Basic Mechanical Properties of Retina in Simple Elongation,” J. Biomech. Eng., **109**(1), pp. 65–67.

[2] Wollensak, G., and Spoerl, E., 2004, “Biomechanical Characteristics of Retina,” Retina, **24**(6), pp. 967–970.

[3] Chen, K., and Weiland, J. D., 2010, “Anisotropic and Inhomogeneous Mechanical Characteristics of the Retina,” J. Biomech., **43**(7).

[4] Chen, K., and Weiland, J. D., 2012, “Mechanical Characteristics of the Porcine Retina in Low Temperatures,” Retina, **32**(4).

[5] Chen, K., and Weiland, J. D., 2014, “Discovery of Retinal Elastin and Its Possible Role in Age-Related Macular Degeneration,” Ann. Biomed. Eng., **42**(3).

[6] Worthington, K. S., Wiley, L. A., Bartlett, A. M., Stone, E. M., Mullins, R. F., Salem, A. K., Guymon, C. A., and Tucker, B. A., 2014, “Mechanical Properties of Murine and Porcine Ocular Tissues in Compression,” Exp. Eye Res., **121**, pp. 194–199.

[7] Qu, Y., He, Y., Zhang, Y., Ma, T., Zhu, J., Miao, Y., Dai, C., Humayun, M., Zhou, Q., and Chen, Z., 2018, “Quantified Elasticity Mapping of Retinal Layers Using Synchronized Acoustic Radiation Force Optical Coherence Elastography,” Biomed. Opt. Express, **9**(9).

[8] Qu, Y., He, Y., Saidi, A., Xin, Y., Zhou, Y., Zhu, J., Ma, T., Silverman, R. H., Minckler, D. S., Zhou, Q., and Chen, Z., 2018, “In Vivo Elasticity Mapping of Posterior Ocular Layers Using Acoustic Radiation Force Optical Coherence Elastography,” Investig. Ophthalmol. Vis. Sci., **59**(1).

[9] He, Y., Qu, Y., Zhu, J., Zhang, Y., Saidi, A., Ma, T., Zhou, Q., and Chen, Z., 2019, “Confocal Shear Wave Acoustic Radiation Force Optical Coherence Elastography for Imaging and Quantification of TheIn Vivo Posterior Eye,” IEEE J. Sel. Top. Quantum Electron., **25**(1).

[10] Pekel, G., Aɫladioɫlu, K., Acer, S., Bozkurt, K., Çetin, E. N., and Yaɫci, R., 2015, “Evaluation of Ocular Elasticity in High Myopia,” Optom. Vis. Sci., **92**(5).

[11] Pekel, G., Aɫladioɫlu, K., Acer, S., Yaɫci, R., and Kaşikçi, A., 2015, “Evaluation of Ocular and Periocular Elasticity after Panretinal Photocoagulation: An Ultrasonic Elastography Study,” Curr. Eye Res., **40**(3).

[12] Tang, J., and Liu, J., 2012, “Ultrasonic Measurement of Scleral Cross-Sectional Strains during Elevations of Intraocular Pressure: Method Validation and Initial Results in Posterior Porcine Sclera,” J. Biomech. Eng., **134**(9), p. 91007.

[13] Cruz Perez, B., Pavlatos, E., Morris, H. J., Chen, H., Pan, X., Hart, R. T., and Liu, J.,

2016, “Mapping 3D Strains with Ultrasound Speckle Tracking: Method Validation and Initial Results in Porcine Scleral Inflation,” Ann. Biomed. Eng., **44**(7).

[14] Ma, Y., Pavlatos, E., Clayson, K., Pan, X., Kwok, S., Sandwisch, T., and Liu, J., 2019, “Mechanical Deformation of Human Optic Nerve Head and Peripapillary Tissue in Response to Acute IOP Elevation,” Invest. Ophthalmol. Vis. Sci., **60**, pp. 913–920.

[15] Ma, Y., Kwok, S., Sun, J., Pan, X., Pavlatos, E., Clayson, K., Hazen, N., and Liu, J., 2020, “IOP-Induced Regional Displacements in the Optic Nerve Head and Correlation with Peripapillary Sclera Thickness,” Exp. Eye Res., **200**.

[16] Ma, Y., Pavlatos, E., Clayson, K., Kwok, S., Pan, X., and Liu, J., 2020, “Three-Dimensional Inflation Response of Porcine Optic Nerve Head Using High-Frequency Ultrasound Elastography,” J. Biomech. Eng., **142**(5), pp. 1–7.

[17] Kallel, F., and Ophir, J., 1997, “A Least-Squares Strain Estimator for Elastography,” Ultrason. Imaging, **19**(3), pp. 195–208.

[18] Fortune, B., Yang, H., Strouthidis, N. G., Cull, G. A., Grimm, J. L., Downs, J. C., and Burgoyne, C. F., 2009, “The Effect of Acute Intraocular Pressure Elevation on Peripapillary Retinal Thickness, Retinal Nerve Fiber Layer Thickness, and Retardance,” Investig. Ophthalmol. Vis. Sci., **50**(10), pp. 4719–4726.

[19] Schuman, J. S., Hee, M. R., Puliafito, C. A., Wong, C., Pedut Kloizman, T., Lin, C. P., Hertzmark, E., Izatt, J. A., Swanson, E. A., and Fujimoto, J. G., 1995, “Quantification of Nerve Fiber Layer Thickness in Normal and Glaucomatous Eyes Using Optical Coherence Tomography: A Pilot Study,” Arch. Ophthalmol., **113**(5).

[20] Bowd, C., Weinreb, R. N., Williams, J. M., and Zangwill, L. M., 2000, “The Retinal Nerve Fiber Layer Thickness in Ocular Hypertensive, Normal, and Glaucomatous Eyes with Optical Coherence Tomography,” Arch. Ophthalmol.

[21] Weinreb, R. N., Leung, C. K. S., Crowston, J. G., Medeiros, F. A., Friedman, D. S., Wiggs, J. L., and Martin, K. R., 2016, “Primary Open-Angle Glaucoma,” Nat. Rev. Dis. Prim., **2**.

[22] Sigal, I. A., Flanagan, J. G., and Ethier, C. R., 2005, “Factors Influencing Optic Nerve Head Biomechanics,” Invest. Ophthalmol. Vis. Sci., **46**(11), pp. 4189–4199.

[23] Hua, Y., Voorhees, A. P., and Sigal, I. A., 2018, “Cerebrospinal Fluid Pressure: Revisiting Factors Influencing Optic Nerve Head Biomechanics,” Invest. Ophthalmol. Vis. Sci., **59**(1), pp. 154–165.

[24] Feola, A. J., Myers, J. G., Raykin, J., Mulugeta, L., Nelson, E. S., Samuels, B. C., and Ethier, C. R., 2016, “Finite Element Modeling of Factors Influencing Optic Nerve Head Deformation Due to Intracranial Pressure,” Invest. Ophthalmol. Vis. Sci., **57**(4), pp. 1901–1911.

[25] Wang, X., Fisher, L. K., Milea, D., Jonas, J. B., and Girard, M. J. A., 2017, “Predictions of Optic Nerve Traction Forces and Peripapillary Tissue Stresses Following Horizontal Eye Movements,” Investig. Ophthalmol. Vis. Sci., **58**(4), pp. 2044–2053.

[26] Perez, B. C., Pavlatos, E., Morris, H., Chen, H., Pan, X., Hart, R., and Liu, J., 2016, “Mapping 3D Strains with Ultrasound Speckle Tracking: Method Validation and Initial Results in Porcine Scleral Inflation,” Ann. Biomed. Eng., **44**(7), pp. 2302–2312.

[27] Pavlatos, E., Perez, B. C., Morris, H. J., Chen, H., Palko, J. R., Pan, X., Weber, P. A., Hart, R. T., and Liu, J., 2016, “Three-Dimensional Strains in Human Posterior Sclera Using Ultrasound Speckle Tracking,” J. Biomech. Eng., **138**(2), pp. 2101–2109.